

# Are the Perseus-Pisces chain and the Pavo-Indus wall connected?

H. Di Nella<sup>1,2</sup>, W.J. Couch<sup>2</sup>, G. Paturel<sup>1</sup>, Q.A. Parker<sup>3</sup>

<sup>1</sup> *Observatoire de Lyon, F69230 Saint-Genis Laval, FRANCE*

<sup>2</sup> *School of Physics, University of New South Wales, Sydney, NSW 2052, AUSTRALIA*

<sup>3</sup> *Anglo-Australian Observatory, Coonabarabran, NSW 2357, AUSTRALIA*

Received Sept 1995; accepted — —

## ABSTRACT

In this paper we present a new redshift survey undertaken to address the rather interesting question that arises when all the currently available redshift information from the LEDA database is plotted in ‘hypergalactic’ coordinates. A significant empty region was found between the southern Pavo-Indus (PI) wall and the northern Perseus-Pisces (PP) chain. This survey tests the reality of this void which may simply reflect previous poor sampling of the galaxies in this region. Redshifts for a magnitude selected sample of 379 galaxies were obtained covering the four UKST/SERC survey fields: #537, #470, #346, #290 with  $15.5 \leq B_T \leq 17.0$ . All redshifts were obtained with the FLAIR multi-object spectroscopy system on the 1.2 m U.K. Schmidt Telescope at Siding Spring, Australia. Two highly significant density enhancements were found in the galaxy distribution at  $133 \text{ Mpc}$  and  $200 \text{ Mpc}$  ( $H_0 = 75 \text{ km.s}^{-1} \text{ Mpc}^{-1}$ ). We claim that no connexion exists between PP and PI. However, a southern extension of PP was detected and makes the total length of this chain of more than 150 Mpc.

**Key words:** galaxies – catalogue – redshifts – large-scale structures

astro-ph/9611211 26 Nov 1996

## 1 INTRODUCTION

Over recent years, an increasingly detailed picture of the large- scale galaxy distribution of the local ( $d < 200 \text{ Mpc}$ ) universe has emerged with the advent of large systematic redshift surveys (e.g. de Lapparent et al. 1986, Geller and Huchra 1989, Da Costa et al. 1988, Shanks et al. 1994).

Before the compilation of these large redshift surveys, astronomers mapped large-scale structures from the projected 2-D galaxy distribution based on either subjective visual studies (Lick catalogue, Shane & Wirtanen 1967) or more recently from objective machine-based scanning of the available Schmidt sky survey plates (Collins et al. 1992). However, rapid progress with redshift surveys led to more complex 3-D structures being discovered starting with the first discovery of a cell-like structure reported by Joeveer et al. (1978). Later Kirshner et al. (1981) found a very large empty region of galaxies: the so called Bootes void.

Anticipating the growth industry of redshift surveys and their use as a tool to describe the 3-D galaxy distribution, a collaboration between the Observatories of Lyon and Meudon was formed in 1983 to establish the first computer database to record all published information on galax-

ies: LEDA\*. Around this time, the existence of superclusters, voids, filaments and sheets was being confirmed with typical feature scales of  $\sim 50 \text{ Mpc}$ . In 1988, a Flamsteed’s equal area projection of 58,000 galaxies, then available in the LEDA database, suggested the existence of a structure even larger than any previously seen (Bottinelli et al., 1986; Paturel et al., 1988). The structure seemed to connect several superclusters (Perseus- Pisces, Pavo-Indus, Centaurus and the Local Supercluster). The LEDA team calculated the pole of this flattened ‘hypergalactic structure’ to be about  $l = 57 \text{ deg}$ ;  $b = 22 \text{ deg}$  in galactic longitude and latitude respectively. This most populated plane (MPP), also claimed by Tully in 1986 and 1987, is tilted by about ten degrees to the plane of the Local Supercluster (de Vaucouleurs 1953, 1956)  $l = 47 \text{ deg}$ ;  $b = 6 \text{ deg}$ . Lynden-Bell (1991) also noticed this alignment of superclusters on the supergalactic plane via an equal area projection of galaxy positions.

Using the CfA1 redshift survey, De Lapparent, Geller and Huchra (1986) graphically confirmed the existence of voids and discovered a ‘filament’ in the Coma cluster region. Geller and Huchra (1989) showed that this filament

\* Lyon-Meudon Extragalactic Database. **telnet:** lmc.univ-lyon1.fr **login:** leda

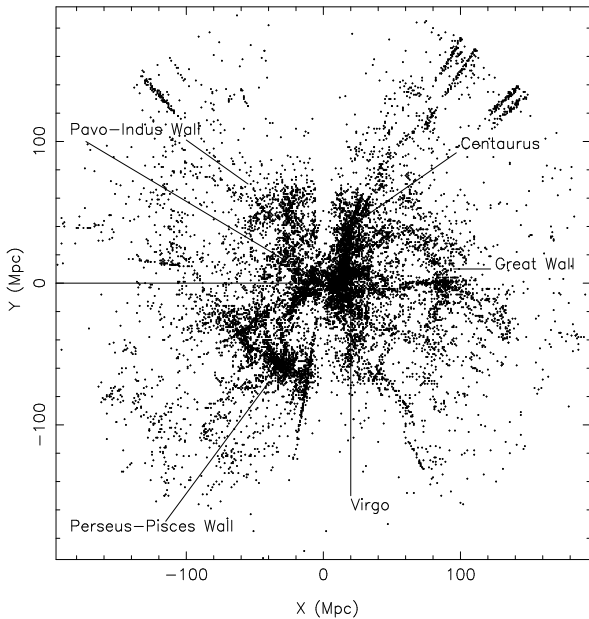


**Figure 1.** Distribution of galaxies from the LEDA sample in a face-on view of the so-called 'hypergalactic' plane (see text). The newly observed region is defined by the two continuous lines.

was actually a sheet-like structure, that has become known as *the Great Wall*, similar to structures predicted in models by Zeldovich (1970). In the southern hemisphere, complementary redshift surveys were undertaken by da Costa et al. (1988) and Fairall et al., (1990). A compilation of available published Southern redshifts by Fairall and Jones, (1991) revealed another wall-like structure in the Pavo-Indus (PI) region. The Perseus-Pisces (PP) region was described either as a chain (Joever et al., 1978; Gregory, Thompson and Tifft, 1981) or a sheet-like structure (Haynes and Giovanelli 1986).

In the 12 years since the inception of LEDA, data for some 100,000 galaxies and more than 36,000 redshifts have been collected. From LEDA a volume-limited ( $v < 15,000 \text{ km.s}^{-1}$ ) and diameter-limited ( $\log D_{25} > 1.2$ ) all-sky sample of 5,863 galaxies was extracted. After studying its completeness in apparent diameter, we used this sample to show that the most populated plane in the local Universe actually coincides with the 'hypergalactic plane or structure' previously found with the Flamsteed 2D-projection (Di Nella and Paturel, 1994 and 1995). If real, this would represent possibly the largest coherent structure in the Universe.

This plane (hereafter the *hypergalactic* plane) is defined by its updated pole and origin in galactic coordinates ( $l(\text{pole}) = 52 \text{ deg}$ ;  $b(\text{pole}) = 16 \text{ deg}$  and  $l(\text{origin}) = l(\text{pole})$ ;  $b(\text{origin}) = b(\text{pole}) - 90 \text{ deg}$ ). To understand the significance of this most populated plane we calculated that at  $\pm 15 \text{ deg}$  around this plane 45% of the sample lay in only 25% of the solid angle. The distribution of the galaxies of the sample is shown in Fig 1.

Despite the wealth of information in Figure 1 there was still a clear need to improve the picture further via additional redshifts. Like the Fairall redshift compilation, the available LEDA redshifts are a collation from a wide variety of sources

all possessing their own selection criteria, biases and errors. Incompleteness in some of these surveys is also occurring just where the walls are becoming populated. Furthermore our azimuthal view is incomplete due to the zones of avoidance in the Milky Way and possible poor sampling in certain directions.

Thus to ascertain whether the great walls seen are part of yet larger shell-like structures we have begun a redshift survey to map the galaxy distribution out through, and beyond the great walls. We hope to determine whether they truly have an outer edge (rather than being an artefact of incomplete data) and also to determine whether the apparent gaps between the walls are real or due to poor sampling. Apart from being pierced by narrow pencil-beam surveys the galaxy distribution beyond the walls has so far been relatively poorly studied.

In this first paper we present results of a new redshift survey in the direction between the Pavo-Indus and Perseus-Pisces walls. This is of particular interest because of the apparent deficiency of galaxies in this direction seen in Figure 1. A prime motivator for studying this region first was to see if there is a possible link between these two major walls as suggested by 2D-projections (Paturel et al., 1988; Santiago et al. 1995).

The paper is organised as follows: in section 2 we describe the selection of the galaxies to be observed, the observing procedure and the data reduction. Section 3 presents the final redshift results whilst the significance of our findings are discussed in section 4.

## 2 OBSERVATIONS

### 2.1 Construction of the sample

To obtain our sample, we want to select galaxies in the empty region between Perseus-Pisces and Pavo-Indus. This region corresponds to the range  $150 \text{ deg} \leq hgl \leq 180 \text{ deg}$  and  $-10 \text{ deg} \leq hgb \leq +10 \text{ deg}$  in hypergalactic longitude and latitude respectively. We decided to limit ourselves in hypergalactic latitude and study only the galaxies lying close to the hypergalactic plane. This would encompass FLAIR observations across 4 UKST/SERC survey fields centered at approximately  $hgb=0 \text{ deg}$  (see Table 2).

From the LEDA database, which contains published data on known galaxies, we selected all galaxies which are positioned in one of the four UKST fields to be observed. Though entries on more than 100,000 galaxies are currently available from LEDA, significant incompleteness exists for a whole range of LEDA galaxy parameters including redshift, magnitude and apparent diameter. Specially, for galaxies fainter than 15.5 B-magnitude, LEDA becomes progressively incomplete.

Thus, it is necessary to complete the LEDA sample from a deeper catalogue. We used the COSMOS database currently 'on line' at the AAO (Drinkwater, Barnes and Ellison, 1995). The COSMOS database consists of parameterised image information for all objects detected above a given isophotal threshold from COSMOS measuring machine scans of the UKST/SERC J survey plates of the whole of the Southern sky (excluding the Milky Way). Star-galaxy separation is provided up to the limiting magnitude for

**Table 1.** Details of the observations

ESO/SERC field #	Set of galaxies	Night of Sept. 1994	Seeing arcsec.	Total exposure time sec.
346	a	6th/7th	2-4	13500
346	a	7th/8th	1-2	9600
537	a	7th/8th	1-2	21000
290	a	8th/9th	2	15000
470	a	8th/9th	2	15000
346	b	9th/10th	1-2	15900
290	b	9th/10th	1-2	7200

galaxies of  $B_T \sim 21$  though sources can be detected up to  $B_T \sim 23$ . However, we only selected galaxies in the range  $15.5 \leq B_T \leq 17$ . This limit, sufficiently deep to provide good sampling at the depths of interest, is a good match to the capabilities of FLAIR and provides a target list that can be observed in reasonable timescales.

Some galaxies fainter than  $B_T = 15.5$  can be present in both LEDA and COSMOS subsamples (see section 2.5). After matching galaxies in both subsamples and rejecting galaxies with known redshift we obtained a total of 905 galaxies for redshift determination as shown in Table 2. Five nights of FLAIR observing time were allocated for the project in September 1994. Even with the fibre multiplex advantage and the capability to observe  $\sim 140$  objects a night by using two FLAIR plateholders it was not possible to observe the total sample of selected galaxies in the nights available. Hence 2 sets of  $\sim 80$  galaxies per UKST field were randomly selected at the rate of 1-in-2 as this gives a good match to the available fibres in each FLAIR plateholder. A final sample of 460 galaxies was obtained.

## 2.2 Observing procedure

The survey was undertaken using FLAIR, the multi-fibre spectroscopy system on the 1.2m UK Schmidt telescope at Siding Spring, Coonabarabran, Australia. FLAIR is ideal for this survey as it combines both a large field of view (6 deg  $\times$  6deg), a large multiplex advantage (73-92 objects simultaneously depending on the FLAIR plateholder used) and a sufficiently faint limiting magnitude ( $B_T \leq 17$ ) to efficiently sample the volume of interest.

The observations, spread over five nights from the 5th to the 9th September 1994, are detailed in Table 1. Unfortunately the first night was lost due to poor weather. The second night was only partly clear with typical seeing of 2-5 arcseconds. The following nights were mostly good with seeing in the range 1-2 arcseconds. Two sets of 80-85 galaxies per field were prepared with the idea of observing two sets of galaxies per night by swapping between the two available plateholders. This was accomplished on three nights but due to weather conditions and some equipment problems half-night exposures were sometimes not enough to obtain data of adequate S/N. In these cases plateholder changeover was delayed to later in the night or to the following night.

The length of a FLAIR exposure is determined mainly by the cosmic ray event rate, typically 2-3 per minute. After 3000 seconds  $\sim 100$  cosmic ray events may be detected resulting in significant clutter of a data frame. Important features in galaxy spectra may thus be compromised. An

upper limit of 3000 seconds exposure was adopted. The typical total exposure time per field was in the range  $3 \times 3000$ s to  $7 \times 3000$ s.  $5 \times 3000$ s are normally considered adequate to obtain spectra of S/N ratio  $\sim 20$ .

The G300B grating was used giving 232 Å/mm or 5.12 Å/pixel (CCD resolution). The 2850Å covered on the CCD at this dispersion was selected for the range 4400Å - 7360Å. This choice provided:

- sufficient spectral coverage to give a good chance of seeing a number of different absorption or emission features in galaxies at different redshifts,
- a high enough dispersion to get reasonable redshift accuracy,
- a minimum spreading of the galaxy light to get an acceptable S/N ratio.

The current FLAIR system has very poor efficiency below 4500 Å, but this problem has recently been addressed by the commissioning of a new back illuminated thinned CCD which offers  $> 3$  times the blue DQE of the previous CCD.

To wavelength calibrate the data, arc exposures were taken either side of a set of field exposures at the given dispersion and grating angle. The extremely stable nature of the floor-mounted FLAIR spectrograph obviates the need for more frequent calibration exposures (e.g. Parker & Watson 1995). Light from a selection of arc lamps is simply reflected off the closed dome. Arc exposures were also taken when we changed plateholders to account for the different fibre-formats, focus values etc. Both Neon and Hg-Cd arcs were combined to provide adequate line coverage over the observed wavelength range.

Flat-field exposures were taken using either the zenith twilight sky or by reflection of a featureless quartz-halogen lamp off a specially provided dome flat-field screen. These exposures are used to obtain the fibre-to-fibre transmission function (see Parker and Watson 1990) vital to ensure proper sky-subtraction. Differences between fibre transmission efficiencies between the twilight sky and dome flats are at the  $\sim 2\%$  level (Parker & Lee, 1994). Bias frames were also taken before and/or after observations in order to correct for any sensitivity variations, cosmetic defects and systematic pixel-to-pixel variations on the CCD. Of the 92 or 72 available fibres (depending on which FLAIR plateholder is used), 5-8 were devoted to the night sky to facilitate satisfactory sky subtraction across the wide field.

## 2.3 Data reduction

All the data reduction was performed using the NOAO IRAF spectral reduction package together with a few additional FLAIR specific IRAF tasks. A FLAIR IRAF data reduction manual exists to facilitate the process (Drinkwater and Barnes, 1994). It is based mainly on existing IRAF packages for multifiber spectroscopy such as 'dohydra'. The final derivation of the radial velocities was done using the 'rvsao' cross-correlation IRAF package.

The first stage of the process is to combine several bias exposures into a single image; this is required to remove any structure in the bias level across the CCD. It is also necessary to combine the flat field frames used to determine and correct for the relative transmission efficiency of the different fibre apertures. This frame is also used to define and identify the fibre apertures themselves. The next stage

**Table 2.** Selection of the target galaxies

HGB range in deg	HGL range in deg	RA and DEC of field centre	UKST/SERC field number	number of target objects	number of observed objects
-6 +0	174 180	23h50 -25deg	537	199	83
-3 +3	166 172	23h23 -30deg	470	202	85
-3 +3	154 160	22h58 -40deg	346	247	129
-5 +1	149 155	22h52 -45deg	290	257	163

is to use the IRAF task 'ccdproc'. This task removes the electronic zero level first by subtracting the combined bias image from each frame and secondly by subtracting the average over the columns in the overscan region. Finally the image is trimmed to leave just the part containing useful data. The individual data frames are now combined to increase the S/N ratio of the final spectra. At this stage the cosmic ray events on each frame are effectively removed using a suitable sigma clipping algorithm which rejects pixel whose values deviate significantly from the mean with minimal loss of data. An aperture identification file is then created to specify which apertures are sky and which contain the objects. The FLAIR data are now ready for final processing using the IRAF 'dohydra' task. This complex task was developed for the HYDRA multi-fibre system on the KPNO 4m telescope but can also be effectively used with FLAIR data. From the combined, cleaned and trimmed target frames together with the dome flats and arc exposures, fully reduced dispersion corrected (wavelength calibrated), sky subtracted one dimensional spectra were produced.

#### 2.4 Derivation of radial velocities

The reduced spectra from 'dohydra' can then be input to the IRAF 'rvsao' task to derive the galaxy radial velocities via cross-correlation against filtered templates provided by Q.A. Parker. Such reduction procedures are described in detail by Parker and Watson (1990) and Watson et al. (1991, 1992).

We finally observed 6 sets of  $\sim 80$  galaxies (fields 346 and 290 were observed twice but looking at different galaxies). Among the 460 galaxies observed, 379 gave reliable radial velocities according to a set of strict criteria: ccf peak height cut-off and match between emission and absorption line velocities). An overall success rate of 82% was achieved.

Two fully reduced typical spectra are shown in Figure 2 and Figure 3 for an absorption and emission line spectrum respectively. During the survey a significant number of active galaxies were also identified; they will be reported in a companion paper.

The list of the 379 measured galaxies is given in Table 3 together with COSMOS coordinates and apparent magnitude. These parameters (plus diameter, axis ratio and position angle) were used to perform cross-identification with the PGC/LEDA objects after reduction to the RC3 system (de Vaucouleurs et al., 1990). Both cross correlation results (from 'rvsao') and emission line results (from 'emsao') are presented. A few galaxies with published redshifts were also observed to derive our external error (see section 3).

The columns of Table 3 are arranged as follows:

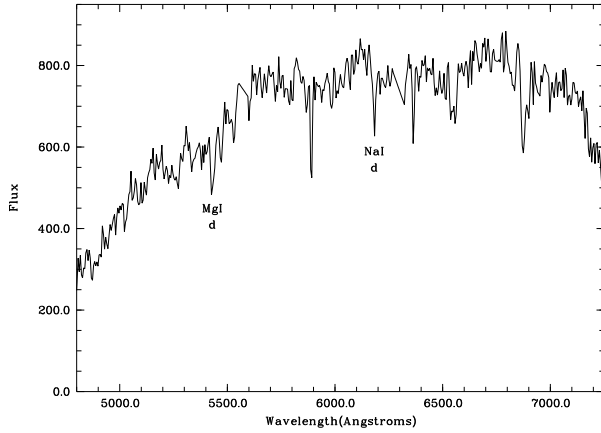


**Figure 2.** Typical reduced absorption line galaxy spectrum (not flux- calibrated) with S/N ratio  $\sim 18.5$ . The vertical axis average counts per exposure ( $1e^- = 1edu$ ). The apparent magnitude is  $B_T = 15.3$ . The combined exposure was  $7 \times 3000s$  and  $V_{helio} = 14772 km.s^{-1}$ .

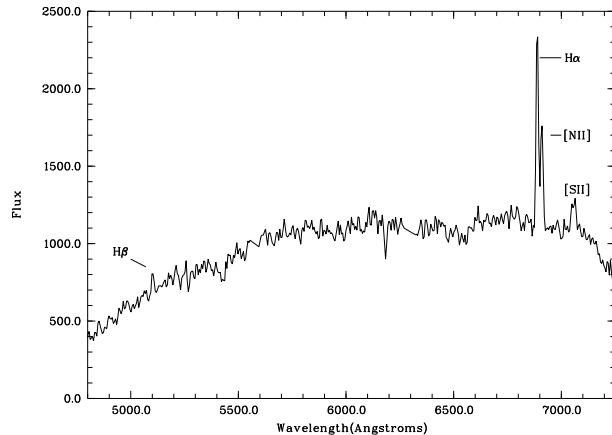


**Figure 3.** Typical reduced emission line galaxy spectrum (not flux calibrated) with  $H_\alpha$ ,  $H_\beta$  and  $S[II]$  lines. The S/N ratio is  $\sim 21$ . The vertical axis is average counts per exposure. The apparent magnitude is  $B_T = 12.6$ . The combined exposure is  $7 \times 3000s$  and  $V_{helio} = 14839 km.s^{-1}$ .

- **column 1:** Right ascension in hours, minutes, seconds, tenths for Equinox 1950.0.
- **column 2:** Declination in degrees, arcminutes and arcseconds for Equinox 1950.0. Coordinates are from the COSMOS database except for a few cases where positions were taken from the LEDA database.
- **column 3:** Internal field number

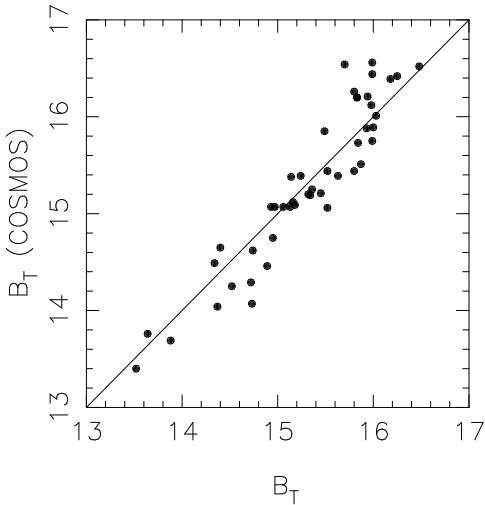


Figure 4. Comparison of galaxy B-magnitudes (see text)

- **column 4:** PGC/LEDA number (Paturel et al. 1989a, b).
- **column 5:** Alternative name in a given hierarchy according to LEDA database: NGC, IC, ESO, MCG, FAIR and DRCG (Dreyer, 1889-1910; Lauberts 1973-1982; Vorontsov-Velyaminov et al. 1962-1974; Fairall 1988, and Dressler 1980).
- **column 6:**  $B_T$  magnitude from COSMOS database after reduction to the LEDA magnitude system (Figure 4):  $B_T = B_{COSMOS} - 0.13$
- **column 7:** Heliocentric velocity  $V_{cc}$  from the cross-correlation method, and its mean error (in  $km.s^{-1}$ ).
- **column 8:** Heliocentric velocity  $V_{em}$  from the emission lines identification method, and its mean error (in  $km.s^{-1}$ )
- **column 9:** notes

## 2.5 Radial velocity external error estimates

To determine the external mean error we made a comparison (Fig 5) between our new measured velocities and those available in LEDA for the few objects in common. This comparison confirms that there is no significant error for the slope or for the zero-point. Rejecting two uncertain measurements, the residual error is  $\sigma=84 km.s^{-1}$ . If we assume that both LEDA and the measurements of this survey have the same mean error, we get a mean error of  $\sigma(V_{cc})=59 km.s^{-1}$ .

The heliocentric velocities measured by the emission line detection method are also compared to published values despite there being only 5 points in common. No slope or zero-point error is found. This is confirmed by a comparison with radial velocities obtained by the cross-correlation method. The mean error is tentatively  $\sigma \approx 180 km.s^{-1}$ .

## 3 RESULTS

The aim of this survey was to study the distribution of galaxies in the region between Perseus-Pisces and Pavo-Indus (see figure 1). With this study we hoped to ascertain whether the apparent gap between these two walls seen in Figure 1 is:

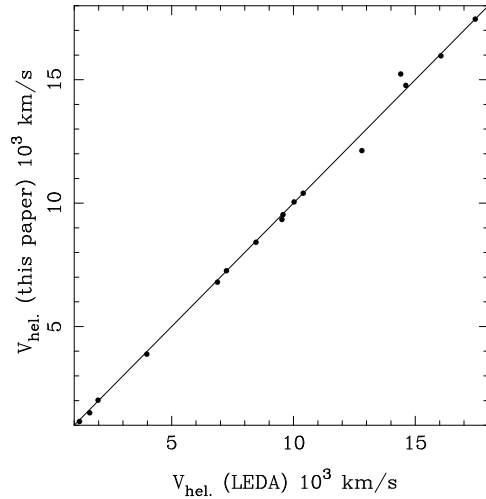


Figure 5. Comparison of new and published heliocentric velocities (see text)

- due to poor sampling of this region by previous surveys, and therefore if there is a link between the Perseus-Pisces and Pavo-Indus Superclusters.
- due to a real void of galaxies.
- due to an ‘apparent’ void of galaxies caused by high-latitude galactic absorption.

To address these questions we first present the new results of this survey in Figure 10. It is important to understand that the plane of this cone diagram is exactly the same as the plane of Figure 1 (the ‘hypergalactic’ or most populated plane). There is evidence of two density enhancements at a radial distance of  $\sim 133$  and  $\sim 200$  Mpc. Their significance seem more clear with the help of a redshift histogram shown in Figure 7. It appears in Figure 11 that these enhancements delineate two low density regions or ‘voids’. When compared to the maps of this region given in the compilation of Fairall & Jones (1991) these voids are real and significant. The nearest one with  $v < 10,000 km.s^{-1}$  is known as the Sculptor Void and the furthest with  $v > 10,000 km.s^{-1}$  was called the Further Sculptor Void by Fairall & Jones. This figure is very interesting because it represents one of the rare regions where two walls perpendicular to the line of sight are seen. We call these ‘chains’ seen from our survey ‘walls’ because they are part of structures which extend above and under the plane of this cone diagram (see Fairall’s catalogue of maps of this region).

When we add these new redshifts to the data of Figure 1, no evidence of a link between the northern Perseus-Pisces and the southern Pavo-Indus features can be seen. The current survey sampled at a rate of 1-in-2 is highly significant and thus we conclude that we cannot have ‘missed’ any link if one existed.

The most prominent feature in Figure 11 is the double peaked velocity distribution. The first peak at  $V_{hel} \approx 10,000 km.s^{-1}$  seems to result from galaxies located in a southern extension of the Perseus Pisces wall which now extends over more than 150 Mpc. The second peak is located at  $V_{hel} \approx 15,000 km.s^{-1}$ .

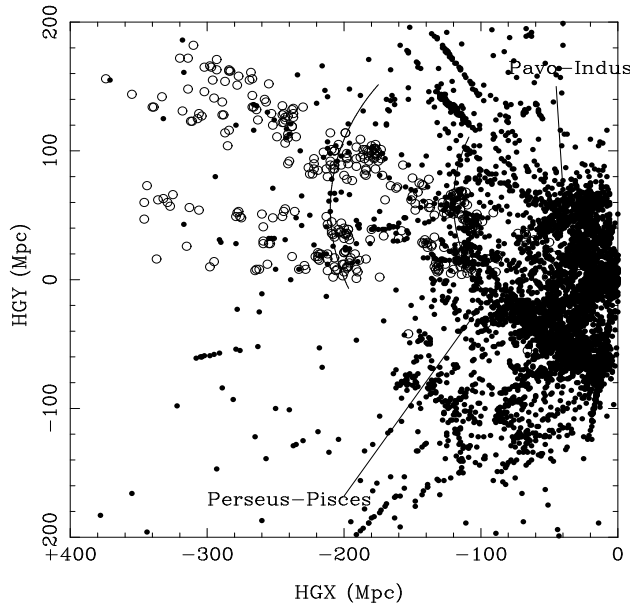


**Figure 6.** Distribution of galaxies within the region surveyed in this study. The filled circles represent LEDA galaxies previously measured in redshift, the open circles are from this survey. This is a view face-on of the hypergalactic plane plane with the Pavo-Indus wall and Perseus-Pisces chain. The position of the density peaks seen in the velocity histogram are indicated by the circle arcs. One of this velocity peak in the redshift survey shows a southern extension to Perseus-Pisces which now extends over more than 150 Mpc.

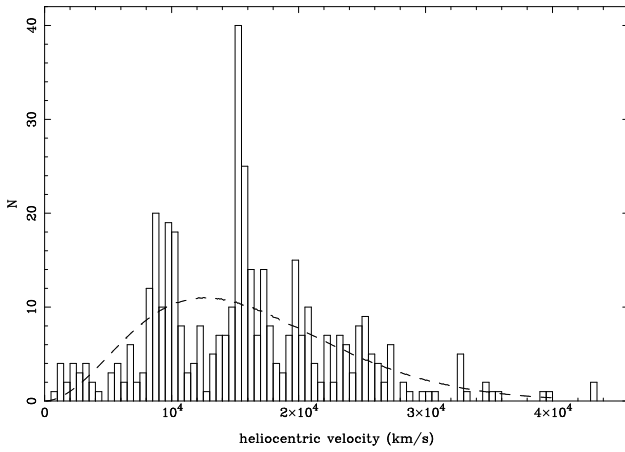


**Figure 7.** Histogram of heliocentric velocities in the studied region. The dashed line represents the selection function of our survey. The most important features are the two highly significant peaks bracketing under-populated regions.

They are compared to the calculated selection function of our survey derived from a standard non- evolving galaxy luminosity function. Because we are claiming that our sample is complete between  $B_T = 15.5$  and  $B_T = 17$ , we calculated the selection function between these limits, using a Schechter function (Schechter and Press, 1976) with the

standard parameters  $M_* = -20$  and  $\alpha = -1.07$ . The function is normalized to our sample total of  $\approx 400$  galaxies.

Assuming Poisson errors, both peaks are significant at a level of  $5\sigma$  and  $11\sigma$ , respectively. It is also clear that the regions corresponding to the Sculptor and the Further Sculptor voids are not consistent with a uniform average space density of galaxies but really are under-populated regions.

#### 4 DISCUSSION AND CONCLUSIONS

One could argue that the observed galaxy distribution is the result of selection effects. Indeed, if our sample was chosen in a biased way, e.g. with more time devoted to a given region at a given distance, one could suspect that the peaks simply reflect the excess of time spent at this distance. Several arguments can be presented against this interpretation.

- Our selection was made on the basis of carefully controlled criteria,  $15.5 \leq B_T \leq 17$ , and without regard to the local density or to distance. Thus, the observed density at a given distance should be representative. In interpreting features of the redshift distribution in this way, one must be extremely worry about the selection effects which bias our view of the structure that is present. For example, could the peaks observed in the velocity distribution simply indicate that our sample is preferentially "tuned" to galaxies at these distances? From the selection function we have computed, the answer in our case is no.

- A completeness test can be made to prove that our sample constitutes a magnitude limited sample with a well defined limit (Figure 8). This diagram has the expected slope of 0.6 indicating that the number of studied galaxies increases, on the mean, as the cube of the distance. For comparison, we plotted on the same figure the completeness curve for the entire sky (normalised to the solid angle of the present survey) obtained from LEDA when imposing that both the apparent magnitude  $B_T$  and the radial velocity  $v$  are known. The completeness limit in the studied region is 1.5 magnitude deeper after our survey.

- Another argument comes from the diagram Figure 6 which shows that the density enhancements are visible in each covered field at the same distance.

- Finally the nearest of the two walls was already visible in the cone diagrams compiled by Fairall and Jones (1991). This wall delineates the Sculptor void and the Further Sculptor void. It is perpendicular to the Sculptor Wall. The furthest wall (at  $15,000 \text{ km.s}^{-1}$ ) has never been noticed before. It delineates the end of the Further Sculptor Void and is perpendicular to the Sculptor Wall.

To continue to address the questions exhibited in section 4 we have explored the map of Burstein & Heiles (1984) to see if a high galactic latitude molecular cloud could be responsible for an apparent void in the distribution of galaxies such as the Sculptor Void. If this was the case, the possibility of a hidden connection between Perseus-Pisces and Pavo-indus could still exist. However we have already a hint: Fairall & Jones didn't see a second wall delimiting the end of the Further Sculptor void, but we did. So it would be very surprising if the galactic absorption could play a role depending on distance i.e. hiding some near galaxies and not some more distant ones. Reinforcing this answer, no mapped

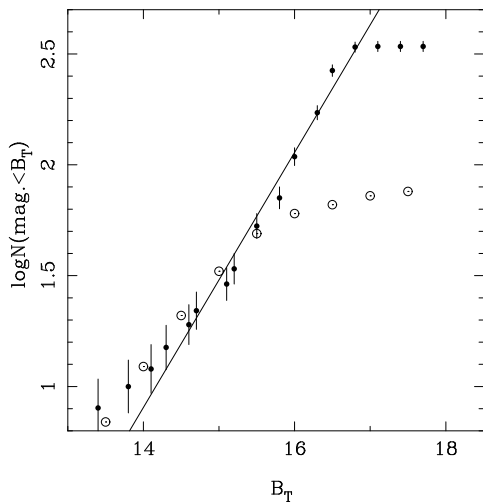


**Figure 8.** Test to show that our sample constitutes a magnitude limited sample with a well-defined cut-off at  $B_T = 17$ . The solid line represents the expected slope 0.6. The mean completeness curve obtained from LEDA for the same solid angle is shown in open circles. A gain of 1.5 magnitude results from our survey.

absorbing cloud is present in the available absorption maps in this direction.

In conclusion, we no longer suspect a link between the Perseus- Pisces and Pavo-Indus walls despite evidences from 2D-projections (Paturel et al., 1988; Santiago et al. 1995). Nevertheless Figure 1 is still a very good representation of our neighbourhood. Updating this figure will be done only by studying the outer regions of the major walls and trying to fill in the missing data across the zones of avoidance. The Further Sculptor Void can now be considered delimited by a wall at  $15,000 \text{ km.s}^{-1}$ , and Perseus-Pisces is extended in the Southern hemisphere. The total length of this chain is now more than 150 Mpc.

## ACKNOWLEDGEMENTS

We are grateful to those who have managed the LEDA extragalactic database over the last 12 years: N. Durand, P. Fouqué, A.M. Garcia, R.Garnier, M. Loulergue, M.C. Marthinet and C. Petit. We are also grateful to those who assisted during the observations: the UKST staff, S. Besier and K. Sealey. We acknowledge the COSMOS/UKST Southern Sky Catalogue supplied by the COSMOS group at the Royal Observatory Edinburgh to the Anglo-Australian Observatory. This work has been supported by grants from the Conseil Régional Rhône-Alpes (F) and by the Institut National des Sciences de l'Univers (F). We thank the University of New South Wales for welcoming us and for providing us the facilities with which we have conducted this study. Q.A. Parker is on special leave from the ROE to work at the AAO. We thank the referee for his comments.

## REFERENCES

Bottinelli L., Gouguenheim L., Fouqué P., Paturel G., 1986, in *La Dynamique des Structures Gravitationnelles*, Observatoire de Lyon

Burstein and Heiles, 1984, *ApJ Suppl.* 54, 33

Da Costa L.N., Pellegrini P.S., Sargent W.L.W., Tonry J., Davis M., Meiksin A., Latham D.W., Menzies J.W., Coulson I.A., 1988, *ApJ* 327, 544

Di Nella H. and Paturel G., *Comptes rendus de l'académie des sciences, série II*, t319, p57-62, 1994

Di Nella H. and Paturel G., *Proceedings of the Astronomical Society of Australia*, vol.12, 56, 1995

Dressler, A., 1980, *Astrophys. J. Suppl. Ser.*, **42**, 565

Dreyer, J.L.E., 1889, *MNRAS* **49**,1 (NGC)

Dreyer, J.L.E., 1910, *MNRAS* **59**,105 (IC)

Drinkwater, M.J., Barnes, D.G., Ellison, S.L, 1995, *Publ. Astron. Soc. Aust.* 12, 248

Einasto, J., Corwin, H.G., Huchra, J., Miller, R.H., Tarenghi, M., 1983, *Highlights of Astronomy*, Vol. 6, ed. R. West, Reidel, Dordrecht, p. 757

Einasto, M., Einasto, J., Tago, E., Dalton, G.B. and Andernach, H., 1994, *Mon. Not. R. astr. Soc.*, **269**, 301 (EETDA)

Fairall, A., 1988, *MNRAS* **233**,691 (FAIR)

Fairall A., Jones A., Southern Redshifts Catalogue & Plots, 1991, Publications of the Department of Astro. 11

Fairall A.P., Palumbo G.G.C., Vettolani G., Kauffmann G., Jones A., Baiesi-Pillastrini G., 1990, *MNRAS* **247**, 21P

Geller M., Huchra J., 1988, *Science* 246, 897

Gregory S.A., Thompson L.A., Tifft W., 1981, *ApJ* 243,411

Haynes M.P., Giovanelli R., 1986, *ApJ* 306,L55

Joeveer M., Einasto J., Tago E., 1978, *MNRAS* **185**, 357

Kirshner R.P., Oemler A., Schechter P.L., Shectman S.A., 1981, *ApJ Lett.* 248, L57

Lapparent V.de, Geller M., Huchra J., 1986, *ApJ* 302, L1

Lauberts, A., 1982, The ESO/Uppsala Survey of the ESO(B) Atlas, European Southern Observatory (ESO)

Lynden-Bell D., 1991 in Clusters and Superclusters Ed. A.C. Fabian, p241

Parker Q.A., Lee D., 1994, AAO document on FLAIR performance

Parker Q.A., Watson F.G., 1990, *A&A Suppl.* 84, 455

Parker Q.A., Watson F.G., 1995, SPIE, vol.2476, 34

Paturel G., Bottinelli L., Gouguenheim L., Fouqué P., 1988, *A&A* 189,1

Santiago B.X., Strauss M.A., Lahav O., Davis M., Dressler A., Huchra J.P., 1995, *ApJ* 446, 457

Shane C.D., Wirtanen C.A., 1967, *Pub. Lick Obs.*, 22, 1

Schechter P., Press W., 1976, *ApJ* 203, 557

Tully R.B., 1986, *ApJ*, 303, 25

Tully R.B., 1987, *ApJ*, 323, 1

Vaucouleurs, G.de, 1953, *Astronomical Journal*, 58, 30

Vaucouleurs, G.de, 1956, *Vistas Astr.*, 2, 1584

Vaucouleurs, G.de, Vaucouleurs, A.de, Corwin, H.G. Jr., Buta, R.J., Paturel, G., Fouqué, P., 1991, *Third Reference Catalogue of Bright Galaxies*, Springer-Verlag (RC3)

Vettolani, G. 1993. In *Astronomy from Wide Field Imaging*, edt. MacGillivray, H.T., in press

Vettolani, G. *Studying the Universe with Clusters of Galaxies*, eds. Böhringer, H. and Schindler, S., MPE Report 256, 1994, 7

Vorontsov-Velyaminov,B.A., Arkipova V.P., Kranogorskaja A.A., 1962-1974, *Morphological Catalogue of Galaxies*, Trudy Sternberg Stat. Astr.Inst. 32,33,34,38,46

Watson F.G., Oates A.P., Shanks T., Hale-Sutton D., 1991, *MNRAS*, 253, 222

Zeldovich Y.B., 1970, *A&A* 5, 84

Table 3: The 379 measured galaxies.

RA	1950	DEC	field	PGC/LEDA	Alternat.	BT	Vcc	Err	Vem	Err	Notes
h	m	s	d	'	"	number	number	name	km/s	km/s	km/s
(1)	(2)	(3)	(4)	(5)	(6)	(7)	(8)	(9)			
223534.39	-453312.0	290a_1				15.52	15343	93	-	-	abs
223606.60	-422352.2	290a_2	PGC069407	ES0345-35		16.39	17211	48	-	-	abs
223617.59	-422803.7	290b_104				16.58	12022	59	12008	53	emi
223625.52	-455528.6	290b_105				16.70	19921	146	19920	54	emi
223638.12	-453403.8	290b_106				16.67	7881	67	-	-	abs
223647.90	-453951.8	290a_8				16.53	15576	37	15574	27	emi
223651.77	-455210.1	290a_7				16.39	10236	28	10401	22	emi
223803.00	-473548.0	290b_108	PGC069476	ES0238-21		17.35	9726	50	-	-	emi Sb
223812.13	-470207.8	290a_11				16.03	9998	56	10146	8	emi
223824.69	-444919.8	290b_109				16.65	15066	81	-	-	abs
223825.80	-452727.1	290a_12				16.30	23925	57	23941	56	emi
223906.86	-443008.5	290a_14				16.20	15057	67	15274	9	abs+emi
223943.49	-431014.0	290b_211	PGC069554	ES0290-4		14.62	9339	65	-	-	abs S0 9522
224013.48	-465357.0	290a_15				16.06	9967	46	10024	10	abs+emi
224029.38	-464004.2	290a_16				16.33	27004	81	-	-	abs
224036.80	-453523.4	290b_212	PGC069589	ES0290-6		13.82	2883	54	2866	16	emi Scd
224039.16	-440930.7	290b_113	PGC069593	ES0290-7		15.20	9531	46	9950	28	emi Sb 9568
224126.66	-445833.4	290a_17				16.52	20948	55	21024	13	emi
224131.61	-454921.9	290b_116	LEDA100667			16.77	13531	50	-	-	abs
224209.03	-471143.8	290b_117				16.86	15440	72	15548	69	emi
224215.45	-473752.0	290b_118				16.96	23453	101	23422	31	abs+emi
224244.22	-411047.1	346a_1	PGC069665	ES0345-50		15.34	1772	77	-	-	abs
224329.89	-462214.1	290a_19				16.30	15438	72	15317	55	emi
224345.51	-440042.2	290b_120	PGC069698	ES0290-11A		16.65	20677	74	-	-	abs
224404.32	-434556.6	290a_20				16.17	20700	136	20717	25	abs+emi
224406.63	-460803.3	290b_122				16.79	15162	74	-	-	abs
224422.09	-465132.3	290a_21				16.37	16284	43	16310	7	abs+emi
224423.80	-380845.2	346b_3				17.00	9218	154	9305	29	emi
224427.63	-453347.7	290b_123				16.83	20426	119	20672	39	abs+emi
224428.59	-415016.2	346b_4				16.07	17438	40	17703	25	emi
224437.73	-462353.2	290b_224				16.88	24537	64	-	-	abs
224510.13	-414032.7	346a_7				16.97	24008	109	23838	100	emi
224513.96	-411603.0	346b_7				16.96	21785	293	21945	13	emi
224526.96	-450637.1	290b_228				16.86	15545	81	-	-	abs
224540.58	-392646.2	346b_93				16.99	2734	36	2790	18	emi
224544.57	-460838.8	290b_129				16.47	11855	23	12000	16	emi
224553.72	-373323.6	346b_10				16.23	8877	57	8635	45	emi
224603.91	-430511.8	290b_131	PGC069776	ES0290-15		16.67	5112	20	5161	17	emi
224612.87	-444348.6	290a_26				16.24	24390	114	-	-	abs
224613.53	-373751.7	346b_12				15.90	8656	25	9045	10	emi
224613.88	-385121.2	346b_92				16.71	9099	26	9177	6	emi
224615.42	-463623.6	290b_132				16.72	24434	95	-	-	abs
224617.76	-401448.3	346b_96				16.49	9763	25	9921	13	emi
224629.95	-451224.9	290b_232				16.74	17916	166	17583	32	emi
224636.90	-374101.5	346a_13				16.30	8740	76	-	-	abs
224648.20	-471413.1	290a_27				16.58	23172	55	-	-	abs
224649.17	-385745.2	346a_14				16.55	11265	95	11326	21	emi
224707.60	-374847.9	346b_14				16.63	8785	104	-	-	abs
224710.25	-383515.5	346a_15				16.37	24750	100	-	-	abs
224710.54	-414229.0	346b_70				16.75	9562	45	9652	3	emi
224719.62	-443529.8	290a_30				16.20	9876	22	9911	23	emi
224722.83	-465029.7	290b_135				16.71	24601	105	24368	51	emi
224722.95	-430254.7	290a_31	PGC069833	ES0290-17		15.57	19980	71	-	-	abs S0
224734.23	-440435.8	290a_32	PGC069843	ES0290-18		15.86	20539	134	-	-	abs+emi
224735.79	-374834.6	346a_16				15.84	8689	82	-	-	abs

Table 3: (continued)

RA	1950	DEC	field	PGC/LEDA	Alternat.	BT	Vcc	Err	Vem	Err	Notes
h	m	s	d	'	"	number	number	name	km/s	km/s	km/s
(1)	(2)	(3)	(4)	(5)	(6)	(7)	(8)	(9)			
224749.02	-453546.5	290b_137	PGC069849	ES0290-20		14.17	15226	77	-	-	abs E
224806.59	-403117.8	346b_16				15.64	10049	52	10037	16	emi
224811.90	-453400.3	290b_238				16.86	26880	46	-	-	abs
224814.78	-465618.0	290a_33				15.65	23289	86	-	-	abs
224816.38	-462421.1	290a_34				16.03	10141	78	-	-	abs+emi
224822.88	-380538.4	346a_18				16.63	24863	149	24989	147	emi
224823.07	-382249.6	346b_18	PGC069864	ES0346-5		16.02	9047	52	9062	79	emi Sa
224857.73	-395214.6	346b_19				16.03	17218	36	17233	18	emi
224903.80	-403351.7	346b_82				16.86	9803	40	9955	23	emi
224915.89	-453839.0	290a_38				16.49	15756	87	-	-	abs
224932.92	-453401.0	290b_141				16.87	23761	69	23875	5	emi
224932.98	-403440.6	346b_81				15.87	9827	45	9896	15	emi
224937.58	-381412.0	346b_20				16.59	8441	64	-	-	abs
224951.23	-454130.7	290a_39				16.29	15128	59	-	-	abs
225001.95	-373652.0	346a_21				16.40	1479	43	1599	41	emi
225006.34	-411148.1	346b_69				16.54	16234	62	16410	3	emi
225007.32	-453844.5	290a_40				16.18	20238	112	-	-	abs
225026.04	-394632.3	346b_21				16.99	16880	102	-	-	abs
225034.21	-390356.7	346b_94	PGC069923	ES0346-7		15.20	863	35	928	17	emi Irr
225041.27	-374722.1	346a_21				17.00	23199	54	-	-	abs
225050.77	-440031.1	290b_142				16.77	21305	68	21473	30	emi
225054.30	-383359.4	346b_22				16.93	12215	102	12230	16	abs
225105.04	-474046.7	290b_143				16.85	25449	187	24754	100	emi
225108.02	-391408.8	346a_23				16.21	24890	50	-	-	abs
225124.23	-402455.8	346a_24				16.07	9470	9	9596	15	emi
225127.88	-444427.5	290a_41				15.98	25034	64	25184	29	emi
225128.79	-393453.7	346b_83	PGC069964	NGC7404		13.89	2017	74	-	-	abs E-So 1964
225130.15	-440356.8	290a_42				16.37	20507	83	-	-	abs
225140.67	-450548.6	290a_43				16.33	15126	38	15071	25	emi
225141.37	-423138.9	346a_25	PGC069973	ES0290-23		16.25	17258	56	17541	23	emi
225141.63	-473426.7	290b_244	PGC069975	ES0239-3		16.62	15054	124	-	-	abs
225210.79	-400906.3	346b_25				15.52	13280	48	-	-	abs
225233.89	-381821.5	346b_26	LEDA70005			14.50	11937	167	12227	234	emi
225247.27	-405519.9	346a_27				15.75	13200	40	13344	44	emi
225254.55	-425514.5	290b_146				16.71	14759	49	-	-	abs
225301.44	-450634.3	290a_47				16.55	20432	51	-	-	abs+emi
225305.55	-450154.7	290a_48				16.12	14837	52	-	-	emi
225310.60	-421803.7	346a_28				16.53	16449	109	-	-	abs
225338.05	-393839.3	346a_30	LEDA89332			16.82	8412	20	8469	9	emi
225405.54	-440139.8	290b_147	PGC070085	IC5267B		13.53	1502	90	-	-	abs 1664
225408.67	-451236.3	290a_49				16.31	12694	131	-	-	emi
225411.75	-425845.9	290b_247				16.82	25206	50	25211	16	emi
225416.91	-465516.7	290a_50				16.18	20431	93	-	-	abs+emi
225433.12	-452618.6	290a_51				16.13	20119	26	20226	13	emi
225501.18	-464709.2	290a_52				16.17	25602	90	25619	119	emi
225505.34	-450411.4	290b_149	PGC070120	ES0290-30		15.20	15738	38	15701	27	emi
225508.77	-374704.7	346a_32	PGC070119	ES0346-20		16.33	8358	12	8425	16	emi
225528.17	-391255.8	346b_88	PGC070138	ES0346-21		15.22	8625	54	8718	29	emi
225528.27	-461512.5	290a_53				16.36	15631	76	16093	44	abs+emi
225537.54	-441931.5	290a_55				16.35	15330	114	-	-	abs
225538.50	-403322.8	346b_76				16.46	10146	74	-	-	abs
225542.03	-475630.5	290b_150	PGC070155	ES0239-5		14.73	5404	38	5564	1	emi
225544.66	-454525.2	290a_56				16.00	21925	64	-	-	abs
225554.22	-452420.6	290b_250				16.32	15407	131	-	-	emi
225557.37	-392554.4	346a_33				16.62	10107	43	10227	30	emi

Table 3: (continued)

RA	1950	DEC	field	PGC/LEDA	Alternat.	BT	Vcc	Err	Vem	Err	Notes
h	m	s	d	'	"	number	number	name	km/s	km/s	km/s
(1)	(2)	(3)	(4)	(5)	(6)	(7)	(8)	(9)			
225610.93	-453932.3	290a_57				16.62	15143	62	-	-	abs
225615.99	-391652.3	346b_89				16.87	10308	90	10394	33	emi
225623.25	-461744.2	290a_58				16.29	14764	70	14604	11	emi
225638.95	-465420.9	290a_59				16.02	10005	127	-	-	abs+emi
225756.39	-373630.9	346a_38				16.11	8361	69	8401	29	emi
225818.70	-462435.3	290b_156				16.72	15877	131	15940	80	emi
225826.79	-402130.4	346a_39				16.88	18063	76	-	-	abs
225852.98	-412404.0	346b_39				16.75	13595	13	13919	16	emi
225902.48	-470619.8	290b_157				16.62	15466	81	-	-	abs
225903.18	-443518.2	290b_257				16.57	15594	83	-	-	abs
225907.41	-405535.0	346b_72	PGC070293	ES0346-24		10.37	10046	31	10196	1	emi
225907.43	-444231.7	290a_60				16.31	15819	47	15729	24	emi
225923.27	-471617.5	290a_61				15.79	10336	32	10416	16	emi
225923.89	-394919.3	346a_42	LEDA70304			16.34	1155	50	1218	30	emi
225925.67	-384736.0	346a_43				16.94	27385	85	-	-	abs
225944.15	-425918.9	290a_63	PGC070317	ES0290-36		16.55	14288	29	14683	10	emi
225956.84	-430008.4	290b_159				16.05	26083	89	-	-	emi
230005.80	-380741.8	346b_44				16.88	8519	22	8565	18	emi
230020.04	-465354.0	290a_66				16.45	25896	75	-	-	abs
230026.77	-400702.0	346a_45				16.92	8492	43	8454	24	emi
230029.80	-413924.1	346b_79	PGC070351	ES0346-29		16.52	15169	79	-	-	abs
230050.58	-443517.1	290a_68				16.16	20512	60	21000	5	abs+emi
230051.48	-464808.9	290b_161	PGC070364	ES0290-40		12.79	5797	58	5885	4	emi
230053.12	-440832.2	290a_69	PGC070365	ES0290-41		16.34	10299	15	10573	16	emi
230122.77	-393156.0	346a_46				15.56	17212	94	17423	200	emi
230126.59	-430026.7	290a_72	PGC070391	FAIR1032		15.62	15230	80	-	-	abs
230127.16	-441610.3	290b_163	PGC070390	ES0290-43A		15.57	16603	101	16741	57	abs+emi
230138.47	-472516.3	290a_74				16.42	25576	109	25584	55	emi
230139.62	-392332.9	346b_46				16.81	1311	67	-	-	abs
230212.45	-375959.1	346b_68				16.93	10696	61	10831	4	emi
230218.23	-460919.4	290a_77				16.50	5711	35	5795	8	emi
230229.02	-404206.9	346b_47				15.80	17143	61	-	-	abs
230231.20	-391859.2	346a_48				16.60	27342	134	-	-	abs
230233.40	-441614.4	290a_78				15.60	15999	52	16238	23	emi
230252.20	-420253.7	346b_71				16.41	20446	67	-	-	abs
230306.77	-425808.3	290a_80				15.91	10616	32	10706	21	emi
230315.41	-414640.9	346a_50				16.07	9974	64	10089	29	emi
230319.21	-464927.0	290a_82	PGC070476	FAIR1034		15.57	10404	60	-	-	abs+emi
230330.12	-403715.4	346b_50				16.93	8504	56	-	-	abs
230407.30	-430959.2	290b_168	PGC070494	ES0290-51		14.20	12125	169	12468	10	emi
230423.74	-375108.2	346a_51				16.93	13564	99	-	-	emi
230426.81	-410948.2	346a_52	PGC070514	ES0346-31		12.34	9800	51	9941	14	emi
230445.12	-400502.0	346b_52				16.46	17978	28	18012	24	emi
230507.12	-444143.4	290b_268	PGC070543	ES0290-53		15.19	8668	82	8688	28	emi
230512.39	-450020.9	290a_84				16.59	22198	71	-	-	abs
230531.31	-380231.6	346b_67	PGC070551	ES0346-32		15.20	8669	84	-	-	abs
230539.32	-465120.1	290a_85				16.55	27356	68	27166	123	abs+emi
230542.58	-403443.0	346a_54				16.86	16869	88	-	-	abs
230553.66	-374741.6	346a_55				16.71	17981	66	-	-	abs
230610.95	-394820.2	346b_78				16.63	5434	32	5393	11	emi
230647.60	-380051.5	346b_55				16.56	22720	161	22837	43	emi
230718.84	-392434.6	346b_57				16.92	17630	112	17736	90	emi
230729.93	-405519.8	346a_58				16.76	11525	66	-	-	abs
230730.37	-382422.3	346b_58				16.87	17834	37	18142	27	emi
230757.59	-392021.2	346a_59				16.53	18170	55	-	-	abs

Table 3: (continued)

RA	1950	DEC	field	PGC/LEDA	Alternat.	BT	Vcc	Err	Vem	Err	Notes
h	m	s	d	'	"	number	number	name	km/s	km/s	km/s
(1)	(2)	(3)	(4)	(5)	(6)	(7)	(8)	(9)			
230805.27	-384418.7	346b_59				16.53	17014	36	16958	13	emi
230807.57	-383459.9	346a_60	PGC070630	ES0346-35		15.52	2272	72	2238	113	emi
230843.33	-405015.8	346a_61				16.65	25782	98	25918	30	emi
230852.11	-393759.6	346b_75				16.56	17871	112	-	-	abs
230853.05	-384726.3	346a_62				16.46	19336	76	-	-	abs
230853.57	-421445.8	346b_62				16.63	16579	62	16506	31	emi
230903.99	-403835.8	346a_63				16.23	11091	41	11081	8	emi
230905.44	-405517.0	346b_63				16.72	16846	132	-	-	abs
230907.16	-404129.4	346b_73				16.77	11183	30	11347	1	emi
230919.99	-311056.9	470a_1				16.86	32638	69	-	-	abs
230928.01	-284211.5	470a_2				16.67	9747	41	-	-	abs
230938.16	-281441.7	470a_3				16.82	21266	45	21364	105	emi
230938.88	-420603.4	346b_64				15.91	12313	49	12553	8	emi
230943.58	-272623.4	470a_5				16.74	24977	68	25043	16	emi
230958.87	-294640.0	470a_6				16.76	26430	59	26593	20	emi
231021.19	-303528.1	470a_7				16.73	8921	54	9058	69	emi
231026.87	-423019.8	346a_66				16.64	1224	12	1284	15	emi
231036.20	-273415.6	470a_9				16.58	15935	88	15960	19	emi
231051.82	-291725.7	470a_10				16.31	12232	91	12229	18	emi
231139.56	-284924.0	470a_13				16.99	21169	54	-	-	abs
231200.48	-303040.8	470a_14				16.48	6685	69	6614	22	emi
231221.36	-282304.2	470a_15				16.31	25689	37	25760	15	emi
231229.63	-275450.6	470a_16				16.61	8436	87	8499	7	emi
231232.69	-315633.5	470a_17	LEDA092795			16.52	10362	172	10114	21	emi
231312.31	-305158.9	470a_19				16.19	18670	162	19112	31	emi
231355.40	-283127.7	470a_20				16.85	25082	107	25032	35	emi
231443.86	-280802.1	470a_21				16.82	26343	47	26343	17	emi
231509.68	-281043.5	470a_22				16.99	8850	21	8941	19	emi
231522.01	-282654.3	470a_23				15.97	23846	106	23832	24	emi
231547.52	-274521.1	470a_24				16.06	15824	51	15884	12	emi
231608.09	-290756.7	470a_28				16.85	15605	93	-	-	abs
231614.20	-290224.1	470a_28				16.92	6848	48	6861	17	emi
231653.77	-294819.0	470a_29				16.94	15091	85	-	-	abs
231717.52	-283408.9	470a_30				16.56	23333	100	23320	15	emi
231743.96	-292233.2	470a_31				16.98	25377	48	25526	17	emi
231803.20	-300813.6	470a_33				16.97	24897	61	24934	8	emi
231813.90	-291350.4	470a_34				16.33	8614	89	8650	18	emi
231839.28	-322809.4	470a_35				16.44	12158	36	12213	14	emi
231900.23	-312442.4	470a_36				16.97	10824	53	10788	29	emi
231952.77	-293318.0	470a_38	PGC071245	NGC7636		14.75	6797	65	-	-	abs
232037.56	-290016.6	470a_39				16.99	32734	103	31080	15	emi
232059.66	-292406.6	470a_40				16.95	15903	57	-	-	abs
232101.62	-301521.5	470a_41				16.16	15331	75	-	-	abs
232116.15	-301655.7	470a_42				16.89	15050	73	15096	12	emi
232148.66	-293539.3	470a_43				15.51	6750	16	6831	15	emi
232218.73	-322138.9	470a_44	LEDA71377			19.02	8573	34	8629	15	emi
232326.75	-320733.8	470a_47	LEDA71425			15.64	18174	65	-	-	abs
232410.25	-282841.2	470a_49				16.97	15707	75	15817	16	emi
232422.87	-292208.7	470a_50				16.36	21249	81	-	-	abs
232427.27	-292622.8	470a_51				16.96	20997	129	-	-	abs+emi
232458.23	-304122.9	470a_52				16.99	10391	29	10456	2	emi
232514.17	-315709.8	470a_53				16.31	18709	39	18817	3	emi
232516.27	-293844.2	470a_54				16.74	15074	42	15027	16	emi
232545.17	-292511.1	470a_55				16.92	20900	36	-	-	abs
232606.16	-294916.2	470a_57	PGC071551	ES0470-9		15.38	15074	70	-	-	abs

Table 3: (continued)

RA	1950	DEC	field	PGC/LEDA	Alternat.	BT	Vcc	Err	Vem	Err	Notes
h	m	s	d	'	"	number	number	name	km/s	km/s	km/s
(1)	(2)	(3)	(4)	(5)	(6)	(7)	(8)	(9)			
232635.24	-303600.0	470a_58				16.54	10385	53	-	-	abs
232647.31	-313930.8	470a_59				16.35	10694	102	10671	38	emi
232652.89	-312010.3	470a_60				16.38	6891	22	6640	42	emi
232656.29	-290625.0	470a_61	PGC071581	IC5326		14.88	7259	34	7265	9	emi
232706.73	-311208.2	470a_62				16.93	16194	62	15967	21	emi
232724.05	-312558.3	470a_63	PGC071601	ES0470-13		15.32	10917	92	11139	22	emi
232738.05	-300849.1	470a_64				16.22	15392	25	15462	34	emi
232754.27	-290524.8	470a_65	PGC071627	ES0470-15		14.59	7204	46	7538	12	emi
232829.86	-292656.5	470a_67				16.35	13772	20	13875	15	emi
232837.91	-320832.6	470a_68				16.34	16015	39	16085	20	emi
232906.84	-311051.1	470a_70				16.72	10863	38	10909	42	emi
232930.69	-275529.2	470a_72				16.91	8251	20	8298	17	emi
232952.34	-302006.9	470a_74				16.56	15499	59	15296	22	emi
233022.23	-312626.3	470a_75				15.94	10693	48	-	-	abs
233045.61	-285601.6	470a_76				16.83	19660	85	19748	8	emi
233057.73	-290244.0	470a_77				16.71	14848	50	15042	38	emi
233100.77	-295918.3	470a_78				16.47	15009	73	-	-	abs
233102.90	-301327.2	470a_79				15.85	15210	75	-	-	abs
233140.82	-322138.7	470a_80	PGC071767	MCG-5-55-25		15.25	13834	56	-	-	abs
233151.06	-274713.8	470a_81				16.71	26163	88	-	-	abs
233201.17	-300546.6	470a_82				16.03	15167	28	15145	11	emi
233240.62	-291503.6	470a_83				16.65	15199	22	15184	16	emi
233304.43	-303641.1	470a_84				16.94	9081	81	9244	40	emi
233305.89	-302119.1	470a_85				16.78	10585	70	10588	17	emi
233308.45	-313521.1	470a_86				16.71	13122	71	13230	10	emi
233328.81	-324656.9	470a_87				16.69	15560	83	-	-	abs
233338.16	-315247.4	470a_88	PGC071871			14.87	18752	49	-	-	abs
233625.56	-255649.6	537a_3	PGC072012	ES0536-14		14.78	9459	45	9452	3	emi
233655.88	-253234.8	537a_4				16.77	14650	49	14719	7	emi
233713.88	-230200.8	537a_6				15.74	7808	29	7911	15	emi
233723.95	-271933.9	537a_7				16.39	19539	79	19306	13	emi
233735.12	-230031.8	537a_8				16.57	7946	46	7997	15	emi
233755.16	-264958.6	537a_9				16.29	15052	59	14860	20	emi
233834.71	-225826.2	537a_10				16.94	14366	56	-	-	abs
233842.73	-251847.4	537a_11				16.71	15611	25	15640	17	emi
233903.62	-253437.0	537a_13				16.06	16456	129	16764	8	emi
233956.30	-271150.4	537a_14				16.63	19235	73	20098	2	emi
234041.77	-252223.9	537a_15				16.73	15936	29	16012	3	emi
234053.73	-262104.7	537a_16	LEDA89427			16.25	15969	25	15895	1	emi
234106.20	-231921.2	537a_17				16.68	9192	44	-	-	abs
234136.42	-244142.4	537a_18				16.64	6703	20	6730	15	emi
234139.33	-262500.7	537a_19				16.94	16380	39	-	-	abs
234147.24	-241554.8	537a_20	PGC072264	ES0537-2		15.27	14355	49	-	-	abs
234155.93	-262828.3	537a_21				16.67	16427	27	16474	15	emi
234201.11	-253029.5	537a_22				16.48	14711	41	14778	13	emi
234202.41	-240517.1	537a_23	PGC072282	ES0537-3		15.33	14772	83	-	-	abs
234234.43	-240517.1	537a_26	PGC072310	ES0537-4		16.74	9817	55	9814	16	emi
234249.50	-271036.8	537a_28				15.78	14488	115	-	-	abs
234252.94	-245311.9	537a_29				16.36	9835	41	-	-	abs
234300.11	-271758.8	537a_30				16.61	15068	67	-	-	abs
234305.94	-252713.7	537a_31				16.61	16447	29	16975	13	emi
234316.60	-240033.2	537a_32	PGC072342	ES0537-7		11.46	9924	82	10257	2	emi
234328.95	-231035.2	537a_33	PGC072349	ES0537-8		16.45	14275	55	-	-	abs+emi
234334.98	-252432.0	537a_34				16.55	9930	65	-	-	abs

Table 3: (continued)

RA	1950	DEC	field	PGC/LEDA	Alternat.	BT	Vcc	Err	Vem	Err	Notes
h	m	s	d	'	"	number	number	name	km/s	km/s	km/s
(1)	(2)	(3)	(4)	(5)	(6)	(7)	(8)	(9)			
234340.60	-260408.5	537a_35	PGC072356	ES0537-9		16.27	8648	47	8632	15	emi
234343.74	-250447.6	537a_36	LEDA89431			16.66	14769	43	14455	16	emi
234352.09	-253829.6	537a_37				16.61	10063	75	-	-	abs
234356.74	-273917.1	537a_38				16.72	15022	24	15116	15	emi
234357.69	-231032.1	537a_39				16.56	8525	16	8588	15	emi
234413.84	-260038.9	537a_40				16.38	9888	56	-	-	abs
234424.35	-231135.0	537a_42	LEDA089433			16.19	17456	22	17546	15	emi
234437.41	-240500.8	537a_43				16.41	22127	22	22091	15	emi
234451.67	-261346.0	537a_44				16.43	9885	70	-	-	abs
234454.36	-275623.8	537a_45	LEDA085761	DRCG54-91		15.88	8605	58	-	-	abs
234503.05	-260533.2	537a_46				16.81	16619	40	16625	18	emi
234507.95	-252632.1	537a_47				16.79	16385	78	-	-	abs
234518.75	-275822.2	537a_48	LEDA085772	DRCG54-90		13.35	15035	22	15007	17	emi
234555.12	-261913.4	537a_49				16.45	23766	53	-	-	abs
234612.35	-275237.2	537a_50	LEDA085791	DRCG54-94		16.69	19581	74	-	-	abs
234619.91	-221809.9	537a_51	PGC072497	NGC7758		15.98	13084	50	-	-	abs
234624.75	-233118.3	537a_52				16.91	17142	50	17105	15	emi
234647.70	-241948.2	537a_53	PGC072524	ES0537-13		12.59	14871	19	14839	15	emi
234710.38	-275845.0	537a_54	LEDA085810	DRCG54-89		16.57	19163	51	19332	15	emi
234720.16	-241813.4	537a_55				16.16	17218	60	-	-	abs
234722.97	-270809.6	537a_56	PGC072550	ES0537-15		15.99	10070	50	-	-	abs
234752.39	-243222.7	537a_57				16.34	14903	54	-	-	abs
234848.07	-243216.4	537a_58				16.65	15567	37	15493	7	emi
234907.63	-260739.9	537a_59	PGC072650	ES0472-1		16.14	3466	57	3701	17	emi
234929.12	-260812.5	537a_60	PGC072676	ES0472-2		16.01	3054	32	3236	12	emi
234932.29	-233844.1	537a_61				16.67	19808	60	-	-	abs
235003.45	-240633.7	537a_62				16.12	15381	113	-	-	abs
235045.23	-253749.4	537a_63				15.75	9976	47	10083	15	emi
235057.61	-233019.8	537a_64				16.43	19883	46	-	-	abs
235107.04	-234009.7	537a_65				16.61	15008	71	15052	20	emi
235135.22	-225343.6	537a_66				16.75	15054	58	15270	18	emi
235152.84	-274757.8	537a_67	PGC072827	ES0471-40		16.33	16526	97	-	-	abs
235205.52	-254600.7	537a_68				16.56	3006	15	3043	15	emi
235210.35	-255704.6	537a_69	PGC072841	ES0472-7		15.64	9071	101	9091	17	emi
235239.90	-240636.9	537a_70	PGC072860	ES0472-10		14.42	3879	29	3962	16	emi
235335.27	-274443.8	537a_72	PGC072933	ES0471-44		15.51	3007	10	3033	15	emi
235357.12	-241302.2	537a_73				16.62	22411	72	22399	17	emi
235439.34	-241818.1	537a_75				16.79	15922	124	15471	17	emi
235458.48	-251216.9	537a_76				16.28	19289	30	19351	15	emi
235522.57	-225944.8	537a_77				16.64	15612	41	15387	6	emi
235645.74	-244315.5	537a_79	PGC073155	ES0472-12		12.99	15493	47	15647	16	emi
235721.40	-273045.0	537a_80	PGC073192	MCG-5-1-21		15.52	8188	33	-	-	abs
235740.23	-252754.4	537a_81				16.67	25403	109	-	-	abs
235740.41	-270032.7	537a_82				16.01	17945	37	-	-	abs
235751.18	-261922.0	537a_83				16.63	15174	53	-	-	abs
235821.95	-261102.4	537a_85				16.39	15065	41	-	-	abs
235837.06	-271755.1	537a_86				16.35	8072	80	8106	17	emi
235848.16	-252826.0	537a_87				16.53	8264	31	8305	4	emi
235922.68	-243335.3	537a_88				16.62	19737	59	19910	16	emi
235956.65	-273428.2	537a_89				16.39	8405	47	-	-	abs
224907.64	-451306.7	290a_37				15.66	16272	81	-	-	emi
225253.11	-423049.6	290a_46				15.69	16455	112	-	-	abs
225536.18	-425446.0	290a_54				16.39	24563	209	-	-	abs+emi
230057.93	-433851.2	290a_70				16.26	10298	110	-	-	emi

Table 3: (continued)

RA	1950	DEC	field	PGC/LEDA	Alternat.	BT	Vcc	Err	Vem	Err	Notes
h	m	s	d	'	"	number	number	name	km/s	km/s	km/s
(1)	(2)	(3)	(4)	(5)	(6)	(7)	(8)	(9)			
223436.88	-462438.1	290b_102				16.64	22297	61	-	-	abs
224854.38	-465122.4	290b_140				16.86	17250	94	-	-	: abs
225235.62	-434501.1	290b_145				16.90	22331	69	-	-	: abs
231552.16	-301437.7	470a_25				16.89	35530	51	-	-	abs
232343.62	-300501.9	470a_48				15.79	19263	66	-	-	abs
232900.98	-325302.1	470a_71	PGC0071670	ES0408-7		15.77	16375	32	-	-	emi
233357.13	-314013.0	470a_90				16.91	19896	87	-	-	abs
235625.27	-233615.2	537a_78				16.57	32558	72	-	-	abs
235755.64	-274005.7	537a_84				16.89	13915	56	-	-	abs
235928.98	-273157.2	537a_89				16.70	14299	95	-	-	abs
224641.29	-374500.7	346b_13	LEDA69800			16.84	8737	52	-	-	abs
225639.21	-385927.7	346b_34				16.93	16150	70	-	-	emi
224315.27	-420427.4	346b_80				16.98	6079	63	-	-	emi
225829.88	-384525.9	346b_90				16.70	15989	82	-	-	emi
225725.28	-401832.0	346a_37				16.68	27170	166	-	-	abs
231030.08	-392516.3	346a_700				16.53	19278	71	-	-	: abs
224341.33	-393252.8	346b_2				16.98	23702	127	-	-	emi
224541.34	-401302.5	346b_8				16.45	2381	74	-	-	emi
225313.90	-380320.5	346b_28				16.93	25193	60	-	-	abs
225600.77	-423943.9	346b_33				16.42	19487	55	-	-	: abs
225747.04	-421705.2	346b_37				16.50	15762	107	-	-	abs
230118.23	-411552.6	346b_45				16.95	9352	72	-	-	: abs
230836.66	-424651.9	346b_60				17.00	5502	87	-	-	: abs
225051.35	-395654.5	346b_65				16.67	10471	57	-	-	: abs
231027.49	-423323.5	346b_85				16.71	15143	63	-	-	: abs
230322.70	-373916.7	346b_91				16.84	11808	85	-	-	abs
224246.17	-401722.0	346b_96	LEDA69667			16.81	5531	93	-	-	: abs
224325.72	-380913.8	346a_2	LEDA85304			16.27	30421	83	-	-	abs
224351.04	-413949.4	346a_3				16.87	17258	92	-	-	abs
224424.69	-373755.7	346a_4				16.71	28788	109	-	-	abs+emi
224431.27	-410847.2	346a_5	LEDA85307			16.57	19960	149	-	-	abs
224453.86	-373842.1	346a_6				16.71	39006	75	-	-	: abs
224927.31	-410128.0	346a_20				16.75	19909	159	-	-	: abs
225655.61	-413516.0	346a_35				16.80	8168	56	-	-	: abs
225905.75	-384549.8	346a_40	LEDA95165			16.46	3799	104	-	-	emi
225947.50	-422755.3	346a_44				16.41	17776	76	-	-	abs+emi
230203.27	-412533.5	346a_47				16.70	19928	125	-	-	abs
231305.70	-403359.5	346a_300	LEDA70869			15.30	15688	70	-	-	: abs
225157.74	-433023.0	290a_55				16.13	39678	68	-	-	abs
225932.57	-460721.7	290a_62				16.87	22748	72	-	-	: abs
223848.59	-424234.0	290b_110				16.38	12093	149	-	-	emi
224510.05	-423259.5	290b_126				16.69	20543	64	-	-	abs
224654.69	-471452.6	290b_134				16.50	33059	105	-	-	abs
225719.05	-465628.1	290b_154				16.92	25180	78	-	-	: abs
224119.08	-452304.8	290b_215	LEDA69621			17.24	32552	83	-	-	abs
224516.82	-461959.9	290b_227				16.29	15401	138	-	-	: abs
225341.41	-472940.1	290b_246				16.78	4339	83	-	-	: abs
225606.30	-461544.0	290b_251				16.82	22051	55	-	-	: abs
000123.74	-232914.1	537a_100				15.50	14388	66	-	-	: abs

Note: the ':' in the notes column indicates a poor determination of the redshift.

'abs' denotes redshift measured from absorption lines

'emi' denotes redshift measured from emission lines